Fast and high-fidelity generation of steady-state entanglement using pulse modulation and parametric amplification

Ye-Hong Chen,[1] Wei Qin,[1] and Franco Nori[1,2]

[1]*Theoretical Quantum Physics Laboratory, RIKEN Cluster for Pioneering Research, Wako-shi, Saitama 351-0198, Japan*
[2]*Department of Physics, University of Michigan, Ann Arbor, Michigan 48109-1040, USA*

We explore an intriguing alternative for a fast and high-fidelity generation of steady-state entanglement. By exponentially enhancing the atom-cavity interaction, we obtain an *exponentially enhanced effective cooperativity* of the system, which results in a high fidelity of the state generation. Meanwhile, we modulate the amplitudes of the driving fields to accelerate the population transfer to a target state, e.g., a Bell state. An *exponentially shortened stabilization time* is thus predicted. Specifically, when the cooperativity of the system is $C = 30$, the fidelity of the acceleration scheme reaches 98.5%, and the stabilization time is about *ten times shorter* than that without acceleration. Moreover, we find from the numerical simulation that the acceleration scheme is robust against systematic and stochastic (amplitude-noise) errors.

I. INTRODUCTION

Quantum entanglement is one of the most striking features of quantum mechanics, and entangled states of matter are now widely used for fundamental tests of quantum theory and applications in quantum information science [1]. Numerous schemes have been proposed to faithfully and controllably generate quantum entangled states [2–5] based on either unitary dynamical evolution [6–16] or dissipative quantum dynamical processes [17–46]. For convenience, we call the last of these "dissipative dynamics" hereafter. Dissipative dynamics, where the dissipation is assumed to be a resource rather than a negative effect, has recently attracted much interest in quantum computation and entanglement engineering. The basic idea of a traditional dissipation-based (TDB) approach is shown in Fig. 1(a). Generally, schemes based on dissipative dynamics are robust against parameter fluctuations, can obtain high-fidelity entanglement with arbitrary initial states, and do not need accurate control of the evolution time.

In a TDB approach, the key point for entanglement generation is to produce a dissipative system such that the target state is a unique steady state, regardless of the initial state [27,39]. This means that the target state is dropped out of the unitary evolution in the effective subspace. The only way to transfer population to the target state is via an uncontrollable and slow dissipation process, and the time required for the entanglement generation is inversely proportional to the decay rates. Usually, high speed and high fidelity cannot coexist in a TDB approach because high fidelity F requires high cooperativity C, according to $(1 - F) \propto 1/\sqrt{C}$ (the optimal value of the fidelity) [18,39], but a high cooperativity means small decay rates. In addition, for most optical systems, it is usually hard to achieve a cooperativity of C larger than 100 [47]. In optical systems, the fast and high-fidelity generation of entangled states in the presence of dissipation is still a challenge in optical systems.

In view of this, we are encouraged to propose a general approach for this problem. The basic idea of our accelerated dissipation-based (ADB) approach is shown in Fig. 1(b). The parametric amplification based on a squeezed-vacuum field [48,49] is used to increase the cooperativity C, and as a result to improve the fidelity F. The couplings connecting the undesired ground (UDG) states and the effective excited state are increased by parametric amplification, but the decays remain unchanged, producing an enhanced cooperativity. Also, the exponential increase of atom-cavity coupling allows us to choose relatively strong driving fields to shorten the evolution time. A pulse modulation based on Lyapunov control [50–58] is used here to induce some additional drivings [the green-dashed arrowed line in Fig. 1(b)]. The additional drivings are designed to accelerate the population transfer from the UDG states to the target state, and they gradually vanish when the population of the target state asymptotically reaches 1. In this case, the system can be rapidly stabilized into the target state, i.e., the steady entangled state.

With current experimental techniques, it is possible to achieve $C \sim 30$ [47,59]. If we consider a relatively good cavity, with cavity decay κ smaller than the atomic decay γ, such as $\kappa \approx 0.3\gamma \approx 0.1g$. Then an evolution time $\geqslant 1500/g$ is necessary to achieve a fidelity of $\sim 96\%$ in the TDB approach. However, by applying our approach, the evolution time is shortened from $1500/g$ to about $160/g$, and the final fidelity is improved from $\sim 96\%$ to $\sim 98\%$. Thus, the fast and high-fidelity generation of steady-state entanglement becomes possible.

This paper is organized as follows. In Sec. II, we show the model and the effective Hamiltonian of the system we consider. In Sec. III, we present the ADB approach to realize a fast and high-fidelity generation of steady-state entanglement. In Sec. IV, we verify the robustness against parameter errors of the scheme by numerical simulation. Conclusions are given in Sec. V.
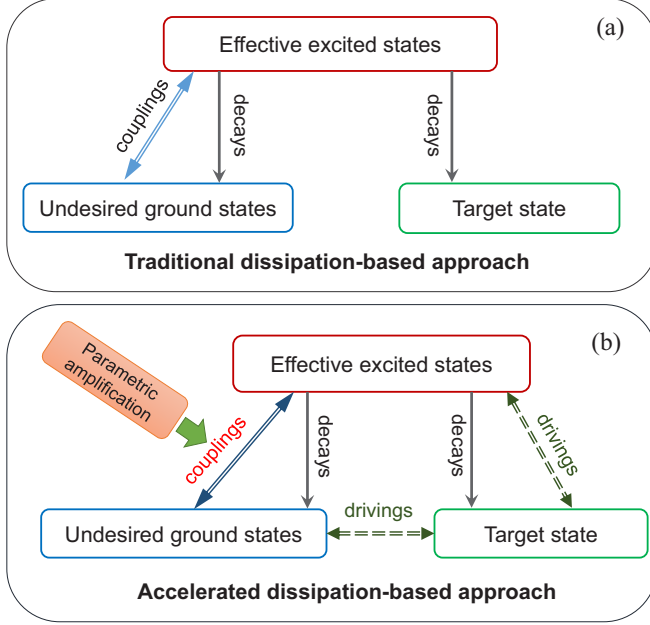
FIG. 1. Schematic of the evolution of a dissipative quantum system in the effective subspace. (a) In a traditional dissipation-based (TDB) approach, the system is well engineered, such that the target state is a unique steady state. (b) In our accelerated dissipation-based (ADB) approach, we use parametric amplification to improve the effective couplings. The (green-dashed arrowed line) additional drivings are induced by pulse modulation, and they are well designed to rapidly increase the population of the target state.

II. MODEL

As shown in Fig. 2(a), we consider a quantum system with two Λ atoms trapped in a single-mode cavity. The level structure of each atom is shown in Fig. 2(b). Note that the pulse modulation is only applied to one of the atoms. The Hamiltonian determining the unitary dynamics of the system, via the rotating wave approximation in a proper observation frame, reads ($\hbar = 1$)

$$H_0 = \sum_{j=1,2} \Delta_e |e\rangle_j \langle e| + H_{\text{AC}} + H_{\text{NL}} + V + H_g,$$

$$H_{\text{AC}} = \sum_{j=1,2} g|e\rangle_j \langle g|a + \text{H.c.},$$

$$H_{\text{NL}} = \Delta_c a^\dagger a + \Omega_p(e^{i\theta_p} a^2 + \text{H.c.}). \quad (1)$$

Here, $V = \sum_{j=1,2} \Omega_j(t) e^{-i\Delta_e t} |e\rangle_j \langle f| + \text{H.c.}$ describes the interaction of a classical laser drive with the atoms; $H_g = \sum_{j=1,2} \Omega_j^{\text{MW}}(t) e^{i\delta t} |f\rangle_j \langle g| + \text{H.c.}$ describes the interaction between the ground states. For brevity, we omit the explicit time dependence of the Hamiltonians H_0, H_g, and V.

By introducing the Bogoliubov squeezing transformation $a_{\text{sc}} = \cosh(r_p)a + e^{-i\theta_p} \sinh(r_p)a^\dagger$, we diagonalize H_{NL} as $H_{\text{NL}} = \omega_{\text{sc}} a_{\text{sc}}^\dagger a_{\text{sc}}$, where

$$r_p = \frac{1}{4} \ln \frac{1+\alpha}{1-\alpha} \quad (2)$$

is the squeezing parameter of the squeezed-cavity mode, and $\omega_{\text{sc}} = \Delta_c \sqrt{1-\alpha^2}$ is the squeezed-cavity frequency ($\alpha =$
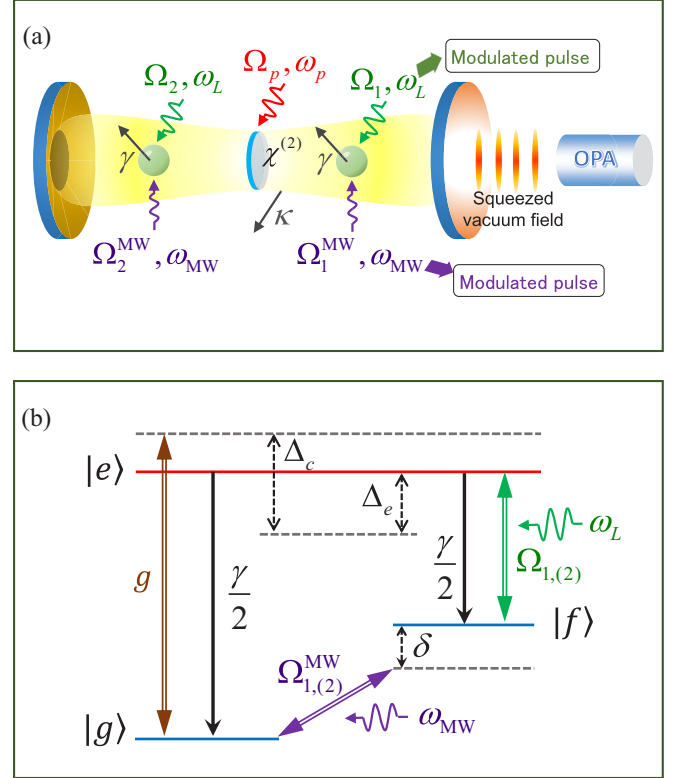

FIG. 2. (a) Schematic diagram of a cavity quantum electrodynamics system containing a single-mode cavity of frequency ω_c, two Λ atoms, a $\chi^{(2)}$ nonlinear medium, and an optical parametric amplifier (OPA). The OPA is used to generate a squeezed-vacuum reservoir which couples to the cavity. Each atom is driven by a laser field and a microwave field with frequencies ω_L and ω_{MW}, respectively. A strong driving field of frequency ω_p is used to pump the nonlinear medium. In addition, with pulse modulation, the amplitudes $\Omega_1(t)$ and $\Omega_1^{\text{MW}}(t)$ are designed to induce the (green-dashed arrowed line) additional drivings in Fig. 1. (b) For each atom, the ground states $|f\rangle$ and $|g\rangle$ are resonantly driven ($\omega_L = \omega_e - \omega_f$) and off-resonantly coupled to the excited state $|e\rangle$ with Rabi frequency $\Omega_j(t)$ and coupling g, respectively. The detunings are $\Delta_e = \omega_e - \omega_g - \omega_p/2$, $\Delta_c = \omega_c - \omega_p/2$, and $\delta = \omega_f - \omega_g - \omega_{\text{MW}}$, respectively, where ω_z is the frequency associated with level $|z\rangle$ ($z = g, f, e$). For convenience, we assume that the spontaneous emission rates are the same for decaying to the $|g\rangle$ and to the $|f\rangle$ states (i.e., $\gamma_f = \gamma_g = \gamma/2$).

$2\Omega_p/\Delta_c$). In this case, when $g \sinh(r_p) \ll (\omega_{\text{sc}} + \Delta_e)$ and $\Delta_e = \omega_{\text{sc}}$, we obtain the exponentially enhanced atom-cavity coupling (see the Appendix for details)

$$g_{\text{sc}} = g \cosh(r_p), \quad (3)$$

and the atom-squeezed-cavity interaction Hamiltonian

$$H'_{\text{AC}} = g_{\text{sc}} \sum_{j=1,2} a_{\text{sc}} |e\rangle_j \langle g| + \text{H.c.} \quad (4)$$

We squeeze the cavity mode to exponentially enhance the atom-cavity coupling, as described above. This can introduce additional noise into the cavity [48,49]. This additional noise can be understood as an effective thermal noise and an effective two-photon correlation. To circumvent

such undesired noise, we introduce a squeezed-vacuum field by an optical parametric amplifier [see Fig. 2(b)], with a squeezing parameter r_e and a reference phase θ_e, to drive the cavity. When choosing $r_e = r_p$ and $\theta_e + \theta_p = \pm(2n+1)\pi$ $(n = 0, 1, 2, \ldots)$, we can completely eliminate this additional noise, as detailed in the Appendix. In this case, the squeezed-cavity mode is equivalently coupled to a thermal reservoir and the additional noise is completely removed. Thus, we can use a standard Lindblad operator to describe the squeezed-cavity decay, i.e., $L_{sc} = \sqrt{\kappa}\, a_{sc}$. The system in this case can be modeled by a master equation in the Lindblad form [60,61]:

$$\dot{\rho} = i[\rho, H_0] + \mathcal{L}(\rho),$$

$$\mathcal{L}(\rho) = \sum_k L_k \rho L_k^\dagger - \frac{1}{2}(L_k^\dagger L_k \rho + \rho L_k^\dagger L_k), \quad (5)$$

where L_k's are the lindblad operators describing a cavity decay $L_{sc} = \sqrt{\kappa}\, a_{sc}$, and four spontaneous emissions $L_{j,z'} = \sqrt{\gamma/2}|z'\rangle_j\langle e|$ $(j = 1, 2, z' = g, f)$. Consequently, increasing r_p enables an exponential enhancement in the cooperativity

$$\frac{C_{sc}}{C} = \cosh^2(r_p). \quad (6)$$

When $r_p > 1$, we have

$$\frac{C_{sc}}{C} \simeq \frac{\exp(2r_p)}{4}. \quad (7)$$

Assuming that the squeezed cavity is initially in the squeezed vacuum state $|0\rangle_{sc}$ and the atoms are initially in their ground states, in the limit of $\Omega_j(t), \Omega_j^{MW}(t) \ll g_{sc}$ [62–68], the evolution of the system is confined to an effective evolution subspace spanned by $|\psi_{gg}\rangle = |gg\rangle|0\rangle_{sc}$, $|\psi_{ff}\rangle = |ff\rangle|0\rangle_{sc}$,

$$|T\rangle = (|fg\rangle + |gf\rangle)|0\rangle_{sc}/\sqrt{2},$$
$$|S\rangle = (|fg\rangle - |gf\rangle)|0\rangle_{sc}/\sqrt{2},$$
$$|D\rangle = (|eg\rangle - |ge\rangle)|0\rangle_{sc}/\sqrt{2}. \quad (8)$$

Meanwhile, the decay process in this subspace can be described by three effective Lindblad operators [39,40,69]

$$\tilde{L}_G = \sqrt{\frac{\gamma}{2}}|\psi_{gg}\rangle\langle D|, \quad \tilde{L}_{T,(S)} = \sqrt{\frac{\gamma}{4}}|T(S)\rangle\langle D|. \quad (9)$$

Here, the cavity mode has been adiabatically eliminated in the limit of $\Omega_j(t), \Omega_j^{MW}(t) \ll g_{sc}$. Note that, here, although in the laboratory frame the squeeze-cavity mode contains a large number of photons, the cavity degree of freedom is adiabatically eliminated in our proposal, resulting in a squeezed-cavity mode mediated coupling between atoms. Thus, our proposal can be potentially extended to implementations of various intracavity quantum operations

III. FAST AND HIGH-FIDELITY ENTANGLEMENT GENERATION

We assume that the Rabi frequencies $\Omega_j(t)$ and $\Omega_j^{MW}(t)$ are

$$\Omega_1(t) = \Omega_0/\sqrt{2} + \Xi_1(t),$$
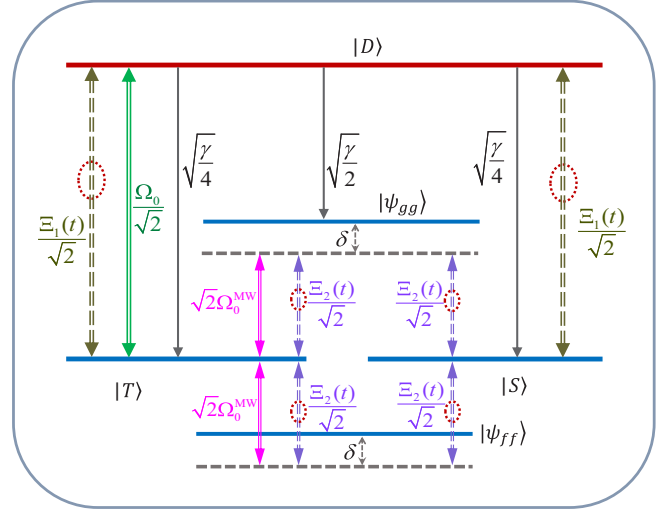$$\Omega_1^{MW}(t) = \Omega_0^{MW}/\sqrt{2} + \Xi_2(t),$$

FIG. 3. The effective transitions for the two-atom system when $\Omega_j(t), \Omega_j^{MW}(t) \ll g_{sc}$. With the effective driving fields and decays, ultimately, the system will be stabilized into the state $|S\rangle$. Here, the red-dotted ellipses represent the control fields induced by the pulse modulation.

$$\Omega_2(t) = e^{i\pi}\Omega_0/\sqrt{2},$$
$$\Omega_2^{MW}(t) = \Omega_0^{MW}/\sqrt{2}, \quad (10)$$

where Ω_0 and Ω_0^{MW} are constants, $\Xi_{1,(2)}(t)$ is the control function of the pulse modulation. We show the effective transitions of the system in Fig. 3. When the pulse modulation is implemented, the evolution process of the system can be described as follows:

(1) The microwave fields $\Omega_j^{MW}(t)$ directly drive the population transfer between the ground states, so that the populations cannot be stored in the UDG states.

(2) Once the population is transferred to the state $|T\rangle$, the modulated driving field $[\Omega_0 + \Xi_1(t)]/\sqrt{2}$ will drive the transition $|T\rangle \to |D\rangle$.

(3) Then, the population in state $|D\rangle$ will be transferred to $|S\rangle$ via the decay $\tilde{L}_S$ and the driving $\Xi_1(t)$.

In this case, by suitably adjusting the control functions $\Xi_j(t)$, we can achieve the target state $|S\rangle$ in a very short time. The shapes of the modulated pulses, as shown in the inset of Fig. 4, are shown to be smooth time-dependent curves that are realizable experimentally. For example, experiments used electro-optic modulators to implement such control fields [70].

Motivated by Lyapunov control theory [51–57], we define the speed of the population increase for a state as the time derivative of its population, i.e.,

$$\mathcal{V}_x(t) = \dot{P}_x(t) = \text{Tr}(\dot{\rho}\rho_x), \quad (11)$$

where $\rho_x = |x\rangle\langle x|$. The rates of the population increase for the ground states are

$$\mathcal{V}_S(t) = \frac{\gamma}{4}\langle D|\rho|D\rangle - i\text{Tr}\{[\rho_S, H_{mod}]\rho\},$$
$$\mathcal{V}_T(t) = \frac{\gamma}{4}\langle D|\rho|D\rangle - i\text{Tr}\{[\rho_T, (H_s + H_{mod})]\rho\},$$
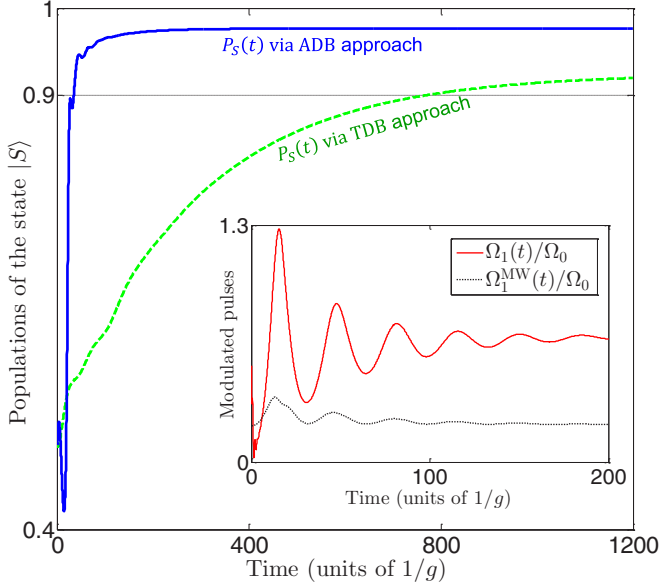
FIG. 4. The population increases of the target state $|S\rangle$ in the ADB approach (blue-solid curve) and in the TDB approach (green-dashed curve). The inset shows the modulated pulses for the ADB approach. The parameters used here are $K_1 = g$, $K_2 = 0.15g$, $r_p = 2$, $\Omega_0 = 0.1g_{sc}$, $\Omega_0^{MW} = 0.2\Omega_0$, $\delta = 0.4\Omega_0$, $\kappa = 0.3\gamma$, and $C = g^2/(\kappa\gamma) = 30$.

$$\mathcal{V}_g(t) = \frac{\gamma}{2}\langle D|\rho|D\rangle - i\mathrm{Tr}\{[\rho_{gg}, (H_s + H_{mod})]\rho\},$$

$$\mathcal{V}_f(t) = -i\mathrm{Tr}\{[\rho_{ff}, (H_s + H_{mod})]\rho\}, \qquad (12)$$

respectively. Here, the Hamiltonian

$$H_s = \frac{1}{\sqrt{2}}\big[\Omega_0|D\rangle + 2\Omega_0^{MW}(e^{i\delta t}|\psi_{gg}\rangle + e^{-i\delta t}|\psi_{ff}\rangle)\big]\langle T| + \mathrm{H.c.} \qquad (13)$$

is the effective Hamiltonian of the system when $\Xi_{1,(2)}(t) = 0$. On account of $H_s|S\rangle = 0$, $\tilde{L}_k|S\rangle = 0$, and $\tilde{L}_k|S\rangle \neq 0$ ($k = L, S, G$), there is a unique steady state, i.e., the target entangled state $|S\rangle$, for the system when $\Xi_{1,(2)}(t) = 0$. The Hamiltonian

$$H_{mod} = \Xi_1(t)H_1 + \Xi_2(t)H_2,$$
$$H_1 = |f\rangle_1\langle e| + |e\rangle_1\langle f|,$$
$$H_2 = |f\rangle_1\langle g| + |g\rangle_1\langle f|, \qquad (14)$$

describes the interaction induced by the pulse modulation. Substituting H_1 and H_2 into Eq. (12), we find the following:

(i) $[\rho_S, H_m] \neq 0$ and $[\rho_T, H_m] \neq 0$ ($m = 1, 2$); both the control functions $\Xi_m(t)$ can adjust the speeds $\mathcal{V}_S(t)$ and $\mathcal{V}_T(t)$;

(ii) $[\rho_{gg}, H_1] = 0$, $[\rho_{gg}, H_2] \neq 0$, $[\rho_{ff}, H_1] = 0$, and $[\rho_{ff}, H_2] \neq 0$; the control function $\Xi_2(t)$ can adjust the speeds $\mathcal{V}_{gg}(t)$ and $\mathcal{V}_{ff}(t)$, while $\Xi_1(t)$ cannot.

These two points indicate that it is hard to design $\Xi_j(t)$ to control one of the speeds in Eq. (12) without influencing the others.

In this case, a simple choice is designing $\Xi_j(t)$ to only control the speed $\mathcal{V}_S(t)$, i.e., the control functions $\Xi_j(t)$ are designed as

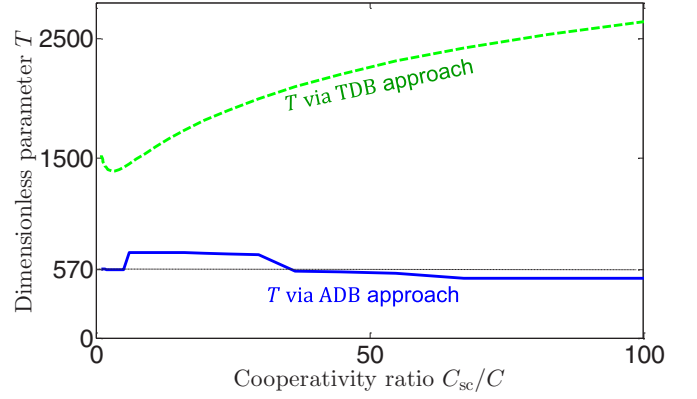$$\Xi_j(t) = -iK_j\mathrm{Tr}\{[\rho_S, H_j]\rho\}, \qquad (15)$$

FIG. 5. The dimensionless parameter $T = (t_S \cdot g_{sc})$ versus the cooperativity ratio $C_{sc}/C = \cosh^2(r_p)$ using different dissipation-based approaches. Here, except r_p, the parameters are the same as the set in Fig. 4.

where $K_j > 0$. Thus, the second term in $\mathcal{V}_S(t)$ is positive, $-i\mathrm{Tr}\{[\rho_S, H_{mod}]\rho\} \geqslant 0$, and the speed $\mathcal{V}_S(t)$ is improved. However, since the driving $\Xi_2(t)$ cannot directly induce an entanglement, designing $\Xi_2(t)$ according to the target state $|S\rangle$ is not the best choice for our goal [71]. In view of this, we have to seek for a new way to design the control function $\Xi_2(t)$.

It is worth noting that the decay causes a relatively fast population increase in the UDG state $|\psi_{gg}\rangle$ according to Eq. (12), and more population will be decayed to the state $|\psi_{gg}\rangle$ than $|S\rangle$ after a certain time evolution. A slow evolution is inevitable to totally transfer the population from the state $|\psi_{gg}\rangle$ to the target state $|S\rangle$. By considering this, the control function $\Xi_2(t)$ can be chosen as

$$\Xi_2(t) = iK_2\mathrm{Tr}\{[\rho_{gg}, H_2]\rho\}, \qquad (16)$$

which is designed to decrease the population of the state $|\psi_{gg}\rangle$ by adding a negative term to the speed $\mathcal{V}_g(t)$. Then, the evolution speeds $\mathcal{V}_S(t)$ and $\mathcal{V}_g(t)$ read

$$\mathcal{V}_S(t) = \frac{\gamma}{4}\langle D|\rho|D\rangle + \frac{|\Xi_1(t)|^2}{K_1} - i\Xi_2(t)\mathrm{Tr}\{[\rho_S, H_2]\rho\},$$

$$\mathcal{V}_g(t) = \frac{\gamma}{2}\langle D|\rho|D\rangle - \frac{|\Xi_2(t)|^2}{K_2} - i\mathrm{Tr}\{[\rho_{gg}, H_s]\rho\}, \qquad (17)$$

respectively. Due to $[\rho_S, H_2] \neq 0$, the last term in $\mathcal{V}_S(t)$ may have a negative effect on the evolution speed, but we can adjust the parameters K_1 and K_2 to minimize this negative effect.

A comparison between the TDB method and the ADB approach is shown in Fig. 4. It takes a very short time (about $110/g$) in the ADB approach to generate the target state with population $\sim 90\%$, while it takes a much longer time (about $780/g$) in the TDB scheme. In the ADB approach, when $t \geqslant t_S = 160/g$, the system gradually becomes stable. The time t_S is called the "stabilization time,' and it describes the time when the system becomes stable. Here, the stabilization is determined according to $\mathcal{V}_S(t_S) \to 0$ and $\dot{\mathcal{V}}_S(t_S) \to 0$. Specifically, in this paper, we assume that when $\mathcal{V}_S(t_S) \leqslant 10^{-5}g$ and $\dot{\mathcal{V}}_S(t_S) \leqslant 10^{-6}g^2$, the system is stable.

TABLE I. Comparison between schemes with and without pulse modulation and parametric amplification. Note the very significant decrease in the stabilization time t_S and the increase in the fidelity F.

Dissipation-based schemes	Squeezing parameter r_p	Cooperativity rate C_{sc}/C	Stabilization time t_S	Fidelity F
Via traditional method	0	1	$\sim 1500/g$	$\sim 96\%$
Via pulse modulation	0	1	$\sim 570/g$	$\sim 95\%$
Via parametric amplification	2	14	$\sim 400/g$	$\sim 98.7\%$
Via our acceleration method	2	14	$\sim 160/g$	$\sim 98.6\%$

For brevity, we define a dimensionless parameter

$$T = t_S \cdot g_{sc}, \tag{18}$$

representing a measurement scale of the stabilization time in the following analysis. As shown in Fig. 5, the dimensionless parameter T in the TDB scheme increases when the amplified cooperativity C_{sc} increases, for example, $T \approx 1500$ when $C_{sc} = 30$, and $T \approx 2500$ when $C_{sc} = 3000$. However, we find the relationship between the stabilization time t_S and the squeezing parameter r_p (see the purple-solid curve in Fig. 6) in our ADB approach is

$$t_S \approx \frac{570}{g \cosh(r_p)} = \frac{570}{g_{sc}}, \tag{19}$$

which means that $T \approx 570$ (see the blue-solid curve in Fig. 5) is independent of the amplified cooperativity C_{sc}. This is an important result of this paper. It predicts an *exponentially shortened stabilization time* t_S when $r_p > 1$. Moreover, the comparison between the TDB approach and the ADB approach in Fig. 5 indicates that the pulse modulation works better in accelerating the evolution when the amplified cooperativity C_{sc} is larger. This means that *the pulse modulation and the parametric amplification supplement each other* in the ADB approach to realize a fast and high-fidelity generation

of steady-state entanglement. This result is also shown in Table I, which shows the comparison between methods with and without pulse modulation and parametric amplification. The improvements in the two bottom rows are very significant. In Table I, the fidelity F is defined as

$$F = \sqrt{\langle S| \rho(t_f) |S\rangle}, \tag{20}$$

where t_f denotes the final time. For convenience, we set $t_f \equiv t_S$ in this paper.

The final population of the state $|S\rangle$ increases when the squeezing parameter r_p becomes larger (see Fig. 6). When $r_p = 3$, the cooperativity is amplified to $C_{sc} \approx 100C = 3000$, and the population of the target state $|S\rangle$ can reach $P_S(t_S) \geqslant 97.5\%$. The stabilization time $t_S = 5/g$ is six times shorter than that in Ref. [48] by only using parametric amplification. Generally, the fidelity of a dissipation-based scheme is higher when r_p is larger. However, a large squeezing parameter r_p corresponds to an extremely strong Ω_p. For example, when $r_p = 3$, the driving field Ω_p reaches $\Omega_p > 10^4 g$, which may cause problems in some experiments. It is better to choose the squeezing parameter $r_p \leqslant 2$ corresponding to $\Omega_p \leqslant 10^2 g$. When $r_p = 2$, the stabilization time becomes $t_S \approx 160/g$, which is almost ten times shorter than that obtained via traditional method as shown in Table I.

IV. ROBUSTNESS AGAINST PARAMETER ERRORS

Influenced by the environment, there are usually two kinds of parameter errors, which should be considered in realizing this approach: systematic error and stochastic error. It is usually hard to avoid errors; for example, the atoms might not be ideally placed. Thus, the various atoms may be subject to slightly different fields, which causes a systematic error. In this case, the actual Hamiltonian should be corrected as $H_n = H_0 + \lambda H_{e1}$, where the subscript "n" represents the "noise," λ is the amplitude of the systematic noise, and H_{e1} is a perturbed Hamiltonian.

When the stochastic error is considered, the actual Hamiltonian becomes $H_n = H_0 + \lambda H_{e1} + \eta H_{e2} \xi(t)$, where $\xi(t) = \frac{\partial}{\partial t} W_t$ is the time derivative of the Brownian motion W_t, η is the amplitude of the stochastic noise, and H_{e2} is also a perturbed Hamiltonian. Since the noise should have zero mean and the noise at different times should be uncorrelated, we have $\langle \xi(t) \rangle = 0$ and $\langle \xi(t) \xi(t') \rangle = \delta(t - t')$. Then, the master equation of the system in the presence of noise is

$$\dot{\rho}_n = -i[H_n, \rho_n] + \mathcal{L}\rho_n$$
$$= -i[H_0, \rho_n] + \mathcal{L}\rho_n - i\lambda[H_{e1}, \rho_n] - i\eta[H_{e2}, \xi(t)\rho_n]. \tag{21}$$
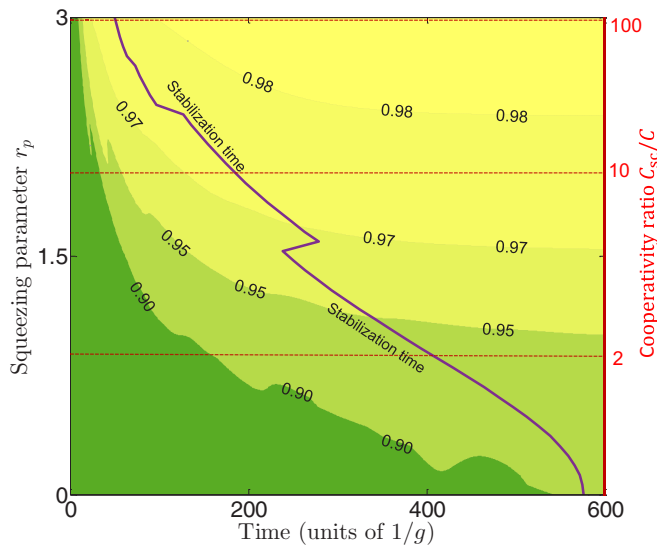

FIG. 6. Contour plot of the population $P_S(t)$ versus time and squeezing parameter r_p in the ADB approach. The red vertical axis (on the right) denotes the cooperativity ratio $C_{sc}/C = \cosh^2(r_p)$. The purple-solid curve represents the time t_S when the system becomes stable. Here, r_p is an independent variable (in the left vertical axis), and other parameters are the same as in Fig. 4.
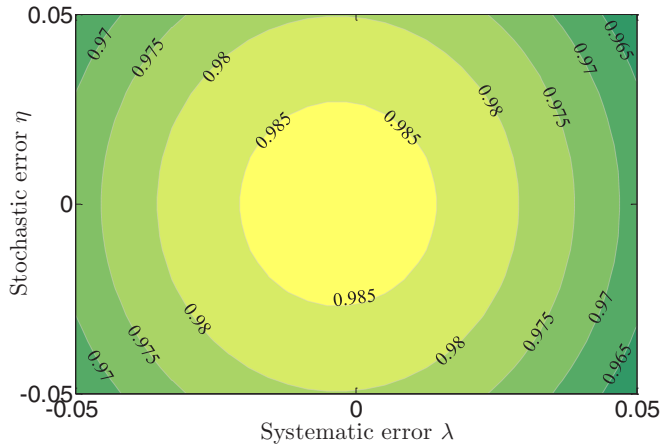
FIG. 7. Contour plot of the fidelity F versus systematic error λ and stochastic error η. Here, the final time is chosen as $t_f = 160/g$, and other parameters are the same as in Fig. 4.

By averaging over the noise, Eq. (21) becomes

$$\dot{\rho}_\mathrm{n} = -i[H_0, \rho_\mathrm{n}] + \mathcal{L}\rho_n - i\lambda[H_{e1}, \rho_\mathrm{n}] - i\eta[H_{e2}, \langle \xi(t)\rho_\mathrm{n}\rangle]. \tag{22}$$

According to Novikov's theorem applied to white noise [72,73], we have

$$\langle \xi(t)\rho_\mathrm{n}\rangle = \frac{1}{2}\left\langle \frac{\delta\rho_\mathrm{n}}{\delta\xi(s)} \right\rangle_{s=t} = -\frac{i\lambda}{2}[H_{e2}, \rho_\mathrm{n}]. \tag{23}$$

We assume the presence of systematic and stochastic (amplitude-noise) errors in $\Omega_1(t)$, so that $H_{e1} = H_{e2} = \Omega_1(t)(|e\rangle_1\langle f| + |f\rangle_1\langle e|)$. For the ADB approach, we can choose $t_f = 160/g$, which is enough for the population P_S to reach $P_S \simeq 97\%$ when $r_p = 2$, as shown above. The systematic error λ has a more serious influence on the fidelity than the stochastic error η, as shown in Fig. 7. A systematic error with intensity $\lambda = 0.05$ causes a deviation of about 1.5% on the fidelity, while a same-intensity stochastic error only causes $\sim0.5\%$ deviation. When $\lambda = \eta = 0.05$, the fidelity is still higher than 96%, which demonstrates that the ADB approach is robust against both systematic and stochastic errors. Beware that the control functions $\Xi_1(t)$ and $\Xi_2(t)$ in H_0 must be given according to the master equation without the noise terms; otherwise, the numerical simulation result in Fig. 7 is possibly wrong.

V. POSSIBLE IMPLEMENTATIONS

In a cavity quantum electrodynamics system, as shown in Fig. 2(a), we consider a possible experimental implementation with ultracold ^{87}Rb atoms trapped in a single-mode Fabry-Perot cavity. The ^{87}Rb atoms can be used for the Λ-type qutrits as shown in Fig. 2(b). Focusing on the D_1 line electric-dipole transitions at a wavelength of 795 nm, the excited state $|e\rangle$ corresponds to the $F' = 2$, $m'_F = -2$ hyperfine state of the $5^2P_{1/2}$ electronic state, and the ground states $|f\rangle$ and $|g\rangle$ correspond to the $F = 1$, $m_F = -1$ and the $F = 2$, $m_F = -1$ hyperfine states of the $5^2S_{1/2}$ electronic ground states, respectively. The transition $|f\rangle \leftrightarrow |e\rangle$ is coupled by a circularly σ^--polarized control laser. The transition $|g\rangle \leftrightarrow |e\rangle$ is
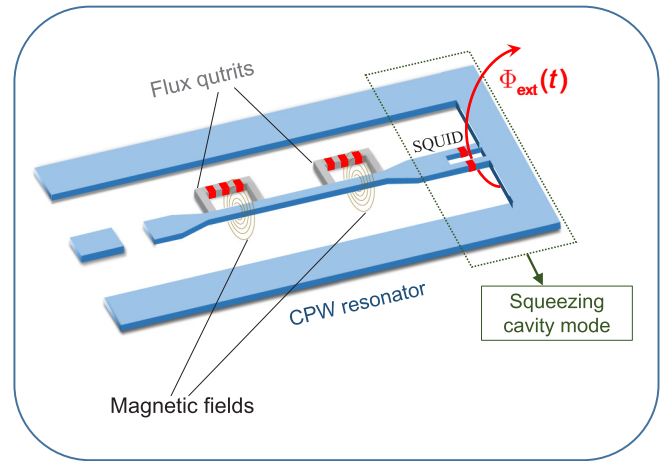

FIG. 8. Schematic diagram representing two flux qutrits coupled a coplanar waveguide (CPW) resonator. The superconducting quantum interference device (SQUID) controlled by the local magnetic flux $\Phi_{\mathrm{ext}}(t)$ threading the loop creates a squeezed vacuum field in the resonator.

coupled by a π-polarized-cavity mode. The transition $|f\rangle \leftrightarrow |g\rangle$ is electric-dipole forbidden, as it is the case for hyperfine levels of alkali atoms. However, a magnetic dipole transition may be used instead, although this may limit the intensity (hundreds of kHz as reported in Refs. [74,75]). In this case, according to the experimental parameters [59], the fidelity of the ADB approach in Sec. III can reach $F \geqslant 98\%$, and the corresponding stabilization time is $t_S \approx 11$ μs.

Another alternative system to realize our approach could be superconducting quantum circuits. Figure 8 shows two flux qutrits coupled a coplanar waveguide (CPW) resonator via the induced magnetic field [76,77]. The necessary squeezing in the resonator is created by inserting a superconducting quantum interference device (SQUID), which is tuned by a magnetic flux $\Phi_{\mathrm{ext}}(t)$ [78–80]. The flux-qubit circuits placed at or near an antinode of the standing wave of the current on the superconducting wire can strongly couple to the superconducting resonator via the mutual inductance [81]. The states $|f\rangle$ and $|e\rangle$ correspond to the first and second excited eigenstates of the flux qubit, respectively. In this system, the transition between $|f\rangle$ and $|g\rangle$ should be much smaller than that between $|e\rangle$ and $|g\rangle$ ($|f\rangle$) so as to guarantee the final stability of the system. This is possible to realize by adjusting the magnetic flux [82–85] in the superconducting circuit system.

VI. CONCLUSION

We investigate the possibility of *simultaneously* improving both the evolution speed *and* the fidelity for a dissipation-based generation of entanglement by pulse modulation and parametric amplification. Regarding two typical dissipation sources in this system: atomic spontaneous emission and cavity decay, we employ atomic spontaneous emission but avoid the effect of cavity decay. The pulse modulation is used to induce two control functions, $\Xi_1(t)$ and $\Xi_2(t)$, where $\Xi_1(t)$ is designed to accelerate the population transfer to the

target state $|S\rangle$, and the $\Xi_2(t)$ is designed to accelerate the population transfer out of the UDG state $|\psi_{gg}\rangle$. The parametric amplification is used to increase the cooperativity, and thus to improve the fidelity of the system. It also allows us to use a relatively large pulse intensity to shorten the stabilization time.

From both analytical and numerical confirmations, we show that the stabilization time in the ADB is *shortened exponentially* with a controllable squeezing parameter r_p. Specifically, when $r_p = 2$, the stabilization time in ADB approach is ten times shorter than that in the TDB scheme, and the fidelity of the ADB approach could reach 98%. We also analyze the sensitivity of the speed-up scheme with respect to systematic and stochastic (amplitude-noise) errors. We find that the ADB approach is robust against parameter errors. Therefore, this alternative method can open venues for the fast and robust realization of high-fidelity entanglement in the presence of dissipation, and can find wide applications in quantum information technologies.

APPENDIX: DERIVATION OF THE EFFECTIVE HAMILTONIAN AND THE LINDBLAD OPERATORS

Squeezing the cavity mode can induce additional noise in the cavity. A possible strategy to suppress such noise is to introduce a squeezed vacuum field, with a squeezing parameter r_e and a reference phase θ_e, to drive the cavity [48]. From the point of view of the cavity, the squeezed input field is well approximated as having infinite bandwidth [86]. In this case, the dynamical evolution of the system in Fig. 2 is modeled by a master equation

$$
\begin{aligned}
\dot{\rho} &= i[\rho, H_0] + \mathcal{L}_a \rho + \mathcal{L}_c \rho, \\
\mathcal{L}_a \rho &= \sum_{k=1}^{4} \mathcal{L}(L_k)\rho, \\
\mathcal{L}_c \rho &= (N+1)\mathcal{L}(L_c)\rho + N\mathcal{L}(L_c^\dagger)\rho \\
&\quad - M\mathcal{L}'(L_c)\rho - M^*\mathcal{L}'(L_c^\dagger)\rho.
\end{aligned}
\tag{A1}
$$

Here, for brevity, we omit the explicit time dependence of ρ and H_0. The subscripts a and c denote the atom and the cavity, respectively. The parameter N is the mean photon number of the broadband squeezed field, and $|M|$ determines the degree of two-photon correlation. The expressions for N and M

are [87,88]

$$
\begin{aligned}
N &= \sinh^2(r_e), \\
M &= \cosh(r_e)\sinh(r_e)\exp(-i\theta_e),
\end{aligned}
\tag{A2}
$$

respectively. Then, the expressions for $\mathcal{L}(o)\rho$ and $\mathcal{L}'(o)\rho$ are

$$
\begin{aligned}
\mathcal{L}(o)\rho &= o\rho o^\dagger - \tfrac{1}{2}(o^\dagger o\rho + \rho o^\dagger o), \\
\mathcal{L}'(o)\rho &= o\rho o - \tfrac{1}{2}(oo\rho + \rho oo),
\end{aligned}
\tag{A3}
$$

where o denotes the Lindblad operator. In the system considered here, there are four Lindblad operators L_k describing the spontaneous emissions:

$$
\begin{aligned}
L_1 &= \sqrt{\gamma/2}|f\rangle_1\langle e|, \quad L_2 = \sqrt{\gamma/2}|f\rangle_2\langle e|, \\
L_3 &= \sqrt{\gamma/2}|g\rangle_1\langle e|, \quad L_4 = \sqrt{\gamma/2}|g\rangle_2\langle e|,
\end{aligned}
\tag{A4}
$$

and one Lindblad operator L_c describing the cavity decay:

$$
L_c = \sqrt{\kappa}\, a.
\tag{A5}
$$

By introducing the Bogoliubov squeezing transformation $a_{\rm sc} = \cosh(r_p)a + e^{-i\theta_p}\sinh(r_p)a^\dagger$, we can diagonalize the nonlinear Hamiltonian $H_{\rm NL}$ as $H_{\rm NL} = \omega_{\rm sc}a_{\rm sc}^\dagger a_{\rm sc}$, where

$$
r_p = \frac{1}{4}\ln\frac{\Omega_p + \Delta_c}{\Omega_p - \Delta_c},
\tag{A6}
$$

is the squeezing parameter, and $\omega_{\rm sc} = \sqrt{\Delta_c^2 - \Omega_p^2}$ is the squeezed-cavity frequency. Accordingly, the atom-cavity coupling Hamiltonian $H_{\rm AC}$ becomes

$$
H_{\rm AC} = \sum_{j=1,2}(g_{\rm sc}a_{\rm sc} - g'_{\rm sc}a_{\rm sc}^\dagger)|e\rangle_j\langle g| + {\rm H.c.},
\tag{A7}
$$

where $g_{\rm sc} = g\cosh(r_p)$ and $g'_s = g\exp(-i\theta_p)\sinh(r_p)$. When $|g'_{\rm sc}| \ll (\omega_{\rm sc} + \Delta_e)$ and $\Delta_e = \omega_{\rm sc}$, the counterrotating terms in Eq. (A7) can be neglected, such that $H_{\rm AC}$ can be transformed to

$$
H'_{\rm AC} = g_{\rm sc}\sum_{j=1,2}a_{\rm sc}|e\rangle_j\langle g| + {\rm H.c.}
\tag{A8}
$$

Meanwhile, the total Hamiltonian in this rotating frame is

$$
\begin{aligned}
H'_0 &= \sum_{j=1,2}\Omega_j(t)|e\rangle_j\langle f| + g_{\rm sc}|e\rangle_j\langle g|a_{\rm sc} \\
&\quad + \Omega_j^{\rm MW}e^{-i\delta t}|f\rangle_j\langle g| + {\rm H.c.}
\end{aligned}
\tag{A9}
$$

The Lindblad term $\mathcal{L}_c\rho$ in Eq. (A1) becomes

$$
\begin{aligned}
\mathcal{L}_c\rho &= (N_{\rm sc}+1)\mathcal{L}(L_{\rm sc})\rho + N_{\rm sc}\mathcal{L}(L_{\rm sc}^\dagger)\rho \\
&\quad - M_{\rm sc}\mathcal{L}'(L_{\rm sc})\rho - M_{\rm sc*}\mathcal{L}'(L_{\rm sc}^\dagger)\rho,
\end{aligned}
\tag{A10}
$$

where $L_{\rm sc} = \sqrt{\kappa}\,a_{\rm sc}$ denotes the squeezed-cavity mode decay, $M_{\rm sc}$ and $N_{\rm sc}$ are

$$
\begin{aligned}
M_{\rm sc} &= e^{i\theta_p}[\sinh(r_p)\cosh(r_e) + e^{-i(\theta_p+\theta_e)}\cosh(r_p)\sinh(r_e)] \\
&\quad \times [\cosh(r_p)\cosh(r_e) + e^{i(\theta_p+\theta_e)}\sinh(r_p)\sinh(r_e)], \\
N_{\rm sc} &= \cosh^2(r_p)\sinh^2(r_e) + \sinh^2(r_p)\cosh^2(r_e) \\
&\quad + \tfrac{1}{2}\sinh(2r_p)\sinh(2r_e)\cos(\theta_p+\theta_e),
\end{aligned}
\tag{A11}
$$

respectively. Then, by choosing $r_e = r_p$ and $\theta_e + \theta_p = \pm(2n + 1)\pi$ ($n = 0, 1, 2, \ldots$), we obtain

$$N_{sc} = M_{sc} = 0. \tag{A12}$$

In this case, the master equation in Lindblad form as shown in Eq. (5) is obtained.

Assuming that the squeezed cavity is initially in the squeezed vacuum state $|0\rangle_{sc}$ and the atoms are initially in their ground states, in the limit of $\Omega_j(t), \Omega_j^{MW}(t) \ll g_{sc}$ [62–67], the evolution of the system is confined to the effective subspace spanned by

$$|\psi_{gg}\rangle = |gg\rangle|0\rangle_{sc}, \quad |\psi_{ff}\rangle = |ff\rangle|0\rangle_{sc},$$

$$|T\rangle = (|fg\rangle + |gf\rangle)|0\rangle_{sc}/\sqrt{2},$$

$$|S\rangle = (|fg\rangle - |gf\rangle)|0\rangle_{sc}/\sqrt{2},$$

$$|D\rangle = (|ge\rangle - |eg\rangle)|0\rangle_{sc}/\sqrt{2}, \tag{A13}$$

where $\{|T\rangle, |S\rangle, |\psi_{gg}\rangle, |\psi_{ff}\rangle\}$ are the basic vectors of the ground-state subspace, and $|D\rangle$ is the dark state of the excited-state subspace. Here $|0\rangle_{sc}$ is a pure single-mode squeezed vacuum state consisting entirely of even-photon Fock state superpositions

$$|0\rangle_{sc} = \frac{1}{\sqrt{\cosh r}} \sum_{n=0}^{\infty} (-\tanh r)^n \frac{\sqrt{(2n)!}}{2^n n!} |2n\rangle. \tag{A14}$$

The even-photon Fock state $|2n\rangle$ obeys $a|2n\rangle = \sqrt{2n}|2n - 1\rangle$ and $a^\dagger|2n\rangle = \sqrt{2n + 1}|2n + 1\rangle$. Single-mode squeezed states are typically generated by degenerate parametric oscillation in an optical parametric oscillator [89], or using four-wave mixing [90].

By modulating the Rabi frequencies as

$$\Omega_1(t) = \Omega_0/\sqrt{2} + \Xi_1(t),$$

$$\Omega_2(t) = e^{i\pi} \Omega_0/\sqrt{2} = \text{constant},$$

$$\Omega_1^{MW}(t) = \Omega_0^{MW}/\sqrt{2} + \Xi_2(t),$$

$$\Omega_2^{MW}(t) = \Omega_0^{MW}\sqrt{2} = \text{constant}, \tag{A15}$$

and the effective Hamiltonian for the system becomes

$$H_{eff} = H_s + H_{mod},$$

$$H_s = \frac{1}{\sqrt{2}}\big[\Omega_0|D\rangle + 2\Omega_0^{MW}(e^{i\delta t}|\psi_{gg}\rangle$$

$$+ e^{-i\delta t}|\psi_{ff}\rangle)\big]\langle T| + \text{H.c.},$$

$$H_{mod} = \frac{1}{\sqrt{2}}[\Xi_1(t)|D\rangle + \Xi_2(t)(e^{i\delta t}|\psi_{gg}\rangle + e^{-i\delta t}|\psi_{ff}\rangle)]\langle T|$$

$$+ \frac{1}{\sqrt{2}}[\Xi_1(t)|D\rangle + \Xi_2(t)(e^{i\delta t}|\psi_{gg}\rangle$$

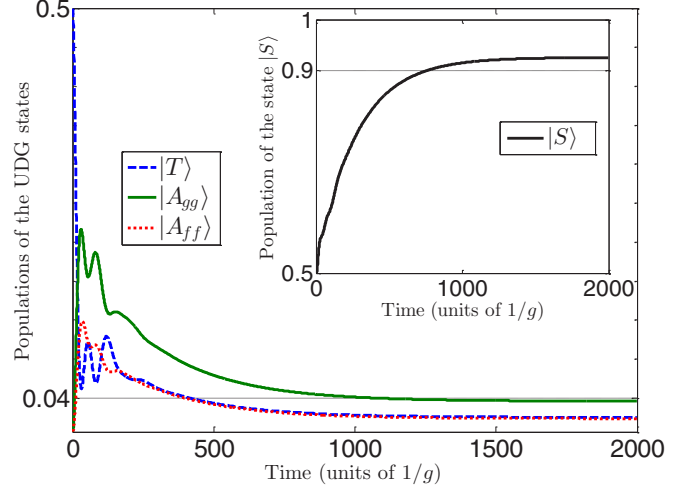$$- e^{-i\delta t}|\psi_{ff}\rangle)]\langle S| + \text{H.c.} \tag{A16}$$

FIG. 9. The populations of the UDG states $|T\rangle$, $|\psi_{gg}\rangle$, and $|\psi_{ff}\rangle$ in the TDB method. The inset shows the population of the target state $|S\rangle$ versus the evolution time. When $t \geqslant 1500/g$, the system becomes stable, i.e., the populations of the ground states gradually become constants. The parameters used here are $\Omega_0 = 0.1g$, $\Omega_0^{MW} = 0.2\Omega_0$, $\delta = 0.4\Omega_0$, $\kappa = 0.3\gamma$, and $C = g^2/(\kappa\gamma) = 30$.

Here, H_{mod} represents the interaction induced by pulse modulation. Accordingly, we obtain the effective Lindblad operators describing the dissipation processes in the effective evolution subspace as

$$\tilde{L}_G = \sqrt{\frac{\gamma}{2}}|\psi_{gg}\rangle\langle D|, \quad \tilde{L}_T = \sqrt{\frac{\gamma}{4}}|T\rangle\langle D|,$$

$$\tilde{L}_S = \sqrt{\frac{\gamma}{4}}|S\rangle\langle D|. \tag{A17}$$

According to the effective Hamiltonian in Eq. (A16) and the effective Lindblad operators in Eq. (A17), we find that, $H_s(\tilde{L}_{k'})|S\rangle = 0$ and $\tilde{L}_{k'}^\dagger|S\rangle = 0$ ($k' = G, T, S$). This means without the pulse modulation ($H_{mod} = 0$), $|S\rangle$ is a steady state of the system. Then, the time evolution of the system can be understood as follows: the microwave fields $\Omega_j^{MW}(t)$ drive the transitions $|\psi_{gg}\rangle \leftrightarrow |T\rangle \leftrightarrow |\psi_{ff}\rangle$, and the laser fields $\Omega_j(t)$ excite $|T\rangle$ to $|D\rangle$, which then decays to $|S\rangle$ via atomic spontaneous emission ($\tilde{L}_S$). In this case, the populations initially in the ground-state subspace are driven to and trapped in $|S\rangle$, resulting in a maximally entangled state $(|fg\rangle - |gf\rangle)/\sqrt{2}$ (see the inset of Fig. 9). Noting that the effective decay rate from $|D\rangle$ to $|\psi_{gg}\rangle$ is two times larger than those from $|D\rangle$ to $|S\rangle$ and $|T\rangle$, the excited state $|D\rangle$ preferentially decays to the ground state $|\psi_{gg}\rangle$ rather than the other ground states. As shown in Fig. 9, the population of the state $|\psi_{gg}\rangle$ increases rapidly to a relatively high level, and then gradually decreases in an oscillating manner. Meanwhile, the populations of the undesired ground states $|T\rangle$ (P_T) and $|\psi_{ff}\rangle$ (P_{ff}) decrease quickly to a negligible level.

[1] S. B. Zheng and G. C. Guo, Efficient Scheme for Two-Atom Entanglement and Quantum Information Processing in Cavity QED, Phys. Rev. Lett. **85**, 2392 (2000).

[2] D. M. Greenberger, M. A. Horne, A. Shimony, and A. Zeilinger, Bell's theorem without inequalities, Am. J. Phys. **58**, 1131 (1990).

[3] W. Dür, G. Vidal, and J. I. Cirac, Three qubits can be entangled in two inequivalent ways, Phys. Rev. A **62**, 062314 (2000).

[4] W. K. Wootters, Entanglement of Formation of an Arbitrary State of Two Qubits, Phys. Rev. Lett. **80**, 2245 (1998).

[5] H.-K. Lo and S. Popescu, Concentrating entanglement by local actions: Beyond mean values, Phys. Rev. A **63**, 022301 (2001).

[6] T. Pellizzari, S. A. Gardiner, J. I. Cirac, and P. Zoller, Decoherence, Continuous Observation, and Quantum Computing: A Cavity QED Model, Phys. Rev. Lett. **75**, 3788 (1995).

[7] J. Pachos and H. Walther, Quantum Computation with Trapped Ions in an Optical Cavity, Phys. Rev. Lett. **89**, 187903 (2002).

[8] A. Beige, D. Braun, B. Tregenna, and P. L. Knight, Quantum Computing Using Dissipation to Remain in a Decoherence-Free Subspace, Phys. Rev. Lett. **85**, 1762 (2000).

[9] E. Solano, G. S. Agarwal, and H. Walther, Strong-Driving-Assisted Multipartite Entanglement in Cavity QED, Phys. Rev. Lett. **90**, 027903 (2003).

[10] A. Serafini, S. Mancini, and S. Bose, Distributed Quantum Computation Via Optical Fibers, Phys. Rev. Lett. **96**, 010503 (2006).

[11] P. B. Li and F. L. Li, Deterministic generation of multiparticle entanglement in a coupled cavity-fiber system, Opt. Express **19**, 1207 (2011).

[12] L. H. Sun, Y. Q. Chen, and G. X. Li, Creation of four-mode weighted cluster states with atomic ensembles in high-q ring cavities, Opt. Express **20**, 3176 (2012).

[13] Z. Q. Yin, F. L. Li, and P. Peng, Implementation of holonomic quantum computation through engineering and manipulating the environment, Phys. Rev. A **76**, 062311 (2007).

[14] M. Lu, Y. Xia, L. T. Shen, J. Song, and N. B. An, Shortcuts to adiabatic passage for population transfer and maximum entanglement creation between two atoms in a cavity, Phys. Rev. A **89**, 012326 (2014).

[15] Y. H. Chen, Y. Xia, Q. Q. Chen, and J. Song, Fast and noise-resistant implementation of quantum phase gates and creation of quantum entangled states, Phys. Rev. A **91**, 012325 (2015).

[16] V. Macrì, F. Nori, and A. F. Kockum, Simple preparation of bell and greenberger-horne-zeilinger states using ultrastrong-coupling circuit qed, Phys. Rev. A **98**, 062327 (2018).

[17] H.-P. Breuer and F. Petruccione, *The Theory of Open Quantum Systems* (Oxford University Press, New York, 2002).

[18] A. S. Sørensen and K. Mølmer, Measurement Induced Entanglement and Quantum Computation with Atoms in Optical Cavities, Phys. Rev. Lett. **91**, 097905 (2003).

[19] G. Vacanti and A. Beige, Cooling atoms into entangled states, New J. Phys. **11**, 083008 (2009).

[20] R. Blatt and D. Wineland, Entangled states of trapped atomic ions, Nature **453**, 1008 (2008).

[21] B. Baumgartner, H. Narnhofer, and W. Thirring, Analysis of quantum semigroups with GKS–Lindblad generators: I. simple generators, J. Phys. A **41**, 065201 (2008).

[22] F. Verstraete, M. M. Wolf, and J. I. Cirac, Quantum computation and quantum-state engineering driven by dissipation, Nat. Phys. **5**, 633 (2009).

[23] K. G. H. Vollbrecht, C. A. Muschik, and J. I. Cirac, Entanglement Distillation by Dissipation and Continuous Quantum Repeaters, Phys. Rev. Lett. **107**, 120502 (2011).

[24] E. G. Dalla Torre, J. Otterbach, E. Demler, V. Vuletic, and M. D. Lukin, Dissipative Preparation of Spin Squeezed Atomic

[25] W. Qin, X. Wang, A. Miranowicz, Z. Zhong, and F. Nori, Heralded quantum controlled-phase gates with dissipative dynamics in macroscopically distant resonators, Phys. Rev. A **96**, 012315 (2017).

[26] D. D. B. Rao and K. Mølmer, Dark Entangled Steady States of Interacting Rydberg Atoms, Phys. Rev. Lett. **111**, 033606 (2013).

[27] F. Reiter and A. S. Sørensen, Effective operator formalism for open quantum systems, Phys. Rev. A **85**, 032111 (2012).

[28] S. Shankar, M. Hatridge, Z. Leghtas, K. M. Sliwa, A. Narla, U. Vool, S. M. Girvin, L. Frunzio, M. Mirrahimi, and M. H. Devoret, Autonomously stabilized entanglement between two superconducting quantum bits, Nature **504**, 419 (2013).

[29] F. Reiter, D. Reeb, and A. S. Sørensen, Scalable Dissipative Preparation of Many-Body Entanglement, Phys. Rev. Lett. **117**, 040501 (2016).

[30] F. Reiter, M. J. Kastoryano, and A. S. Sørensen, Entangled steady-states of two atoms in an optical cavity by engineered decay, New J. Phys. **14**, 053022 (2012).

[31] J. Busch, S. De, S. S. Ivanov, B. T. Torosov, T. P. Spiller, and A. Beige, Cooling atom-cavity systems into entangled states, Phys. Rev. A **84**, 022316 (2011).

[32] L. Memarzadeh and S. Mancini, Stationary entanglement achievable by environment-induced chain links, Phys. Rev. A **83**, 042329 (2011).

[33] A. F. Alharbi and Z. Ficek, Deterministic creation of stationary entangled states by dissipation, Phys. Rev. A **82**, 054103 (2010).

[34] D. Braun, Creation of Entanglement by Interaction with a Common Heat Bath, Phys. Rev. Lett. **89**, 277901 (2002).

[35] X. L. Wang, L. K. Chen, W. Li, H. L. Huang, C. Liu, C. Chen, Y. H. Luo, Z. E. Su, D. Wu, Z. D. Li, H. Lu, Y. Hu, X. Jiang, C. Z. Peng, L. Li, N. L. Liu, Y. A. Chen, C. Y. Lu, and J. W. Pan, Experimental Ten-Photon Entanglement, Phys. Rev. Lett. **117**, 210502 (2016).

[36] L. T. Shen, X. Y. Chen, Z. B. Yang, H. Z. Wu, and S. B. Zheng, Steady-state entanglement for distant atoms by dissipation in coupled cavities, Phys. Rev. A **84**, 064302 (2011).

[37] Y. Lin, J. P. Gaebler, F. Reiter, T. R. Tan, R. Bowler, A. S. Sørensen, D. Leibfried, and D. J. Wineland, Dissipative production of a maximally entangled steady state of two quantum bits, Nature **504**, 415 (2013).

[38] A. W. Carr and M. Saffman, Preparation of Entangled and Antiferromagnetic States by Dissipative Rydberg Pumping, Phys. Rev. Lett. **111**, 033607 (2013).

[39] M. J. Kastoryano, F. Reiter, and A. S. Sørensen, Dissipative Preparation of Entanglement in Optical Cavities, Phys. Rev. Lett. **106**, 090502 (2011).

[40] X. Q. Shao, D. X. Li, Y. Q. Ji, J. H. Wu, and X. X. Yi, Ground-state blockade of Rydberg atoms and application in entanglement generation, Phys. Rev. A **96**, 012328 (2017).

[41] A. Neuzner, M. Körber, O. Morin, S. Ritter, and G. Rempe, Interference and dynamics of light from a distance-controlled atom pair in an optical cavity, Nat. Photon. **10**, 303 (2016).

[42] G. Morigi, J. Eschner, C. Cormick, Y. Lin, D. Leibfried, and D. J. Wineland, Dissipative Quantum Control of a Spin Chain, Phys. Rev. Lett. **115**, 200502 (2015).

[43] H. Krauter, C. A. Muschik, K. Jensen, W. Wasilewski, J. M. Petersen, J. I. Cirac, and E. S. Polzik, Entanglement Generated

Ensembles in a Steady State, Phys. Rev. Lett. **110**, 120402 (2013).

by Dissipation and Steady State Entanglement of Two Macroscopic Objects, Phys. Rev. Lett. **107**, 080503 (2011).

[44] P. B. Li, S. Y. Gao, H. R. Li, S. L. Ma, and F. L. Li, Dissipative preparation of entangled states between two spatially separated nitrogen-vacancy centers, Phys. Rev. A **85**, 042306 (2012).

[45] H. B. Chen, N. Lambert, Y. C. Cheng, Y. N. Chen, and F. Nori, Using non-Markovian measures to evaluate quantum master equations for photosynthesis, Sci. Rep. **5**, 12753 (2015).

[46] J. Ma, Z. Sun, X. G. Wang, and F. Nori, Entanglement dynamics of two qubits in a common bath, Phys. Rev. A **85**, 062323 (2012).

[47] B. Lev, K. Srinivasan, P. Barclay, O. Painter, and H. Mabuchi, Feasibility of detecting single atoms using photonic bandgap cavities, Nanotechnology **15**, S556 (2004).

[48] W. Qin, A. Miranowicz, P. B. Li, X. Y. Lü, J. Q. You, and F. Nori, Exponentially Enhanced Light-Matter Interaction, Cooperativities, and Steady-State Entanglement Using Parametric Amplification, Phys. Rev. Lett. **120**, 093601 (2018).

[49] C. Leroux, L. C. G. Govia, and A. A. Clerk, Enhancing Cavity Quantum Electrodynamics Via Antisqueezing: Synthetic Ultrastrong Coupling, Phys. Rev. Lett. **120**, 093602 (2018).

[50] X. X. Yi, X. L. Huang, C. F Wu, and C. H. Oh, Driving quantum systems into decoherence-free subspaces by Lyapunov control, Phys. Rev. A **80**, 052316 (2009).

[51] D. D'Alessandro, *Introduction to Quantum Control and Dynamics* (Chapman and Hall/CRC, Boca Raton, FL, 2007).

[52] S. Kuang and S. Cong, Lyapunov control methods of closed quantum systems, Automatica **44**, 98 (2008).

[53] S. Kuang and S. Cong, Population control of equilibrium states of quantum systems via Lyapunov method, Acta Autom. Sin. **36**, 1257 (2010).

[54] M. Mirrahimi, P. Rouchon, and G. Turinici, Lyapunov control of bilinear schrödinger equations, Automatica **41**, 1987 (2005).

[55] J. M. Coron, A. Grigoriu, C. Lefter, and G. Turinici, Quantum control design by Lyapunov trajectory tracking for dipole and polarizability coupling, New J. Phys. **11**, 105034 (2009).

[56] Z. C. Shi, X. L. Zhao, and X. X. Yi, Robust state transfer with high fidelity in spin-1/2 chains by Lyapunov control, Phys. Rev. A **91**, 032301 (2015).

[57] W. Cui and F. Nori, Feedback control of Rabi oscillations in circuit QED, Phys. Rev. A **88**, 063823 (2013).

[58] K. Beauchard, J. M. Coron, M. Mirrahimi, and P. Rouchon, Implicit Lyapunov control of finite dimensional Schrödinger equations, Systems & Control Letters **56**, 388 (2007).

[59] C. J. Hood, T. W. Lynn, A. C. Doherty, A. S. Parkins, and H. J. Kimble, The atom-cavity microscope: Single atoms bound in orbit by single photons, Science **287**, 1447 (2000).

[60] A. Kossakowski, On quantum statistical mechanics of non-hamiltonian systems, Rep. Math. Phys. **3**, 247 (1972).

[61] G. Lindblad, On the generators of quantum dynamical semigroups, Commun. Math. Phys. **48**, 119 (1976).

[62] B. Misra and E. C. G. Sudarshan, The Zeno's paradox in quantum theory, J. Math. Phys. **18**, 756 (1977).

[63] W. M. Itano, D. J. Heinzen, J. J. Bollinger, and D. J. Wineland, Quantum Zeno effect, Phys. Rev. A **41**, 2295 (1990).

[64] P. Facchi and S. Pascazio, Quantum Zeno Subspaces, Phys. Rev. Lett. **89**, 080401 (2002).

[65] P. Facchi and S. Pascazio, Quantum Zeno dynamics: Mathematical and physical aspects, J. Phys. A **41**, 493001 (2008).

[66] R. J. Cook, What are quantum jumps? Phys. Scr. **1988**, 49 (1988).

[67] P. Kwiat, H. Weinfurter, T. Herzog, A. Zeilinger, and M. A. Kasevich, Interaction-Free Measurement, Phys. Rev. Lett. **74**, 4763 (1995).

[68] X. B. Wang, J. Q. You, and F. Nori, Quantum entanglement via two-qubit quantum zeno dynamics, Phys. Rev. A **77**, 062339 (2008).

[69] V. V. Albert, K. Noh, and F. Reiter, Dissipative self-interference and robustness of continuous error-correction to miscalibration, arXiv:1809.07324.

[70] Y.-X. Du, Z.-T. Liang, Y.-C. Li, X.-X. Yue, Q.-X. Lv, W. Huang, X. Chen, H. Yan, and S.-L. Zhu, Experimental realization of stimulated raman shortcut-to-adiabatic passage with cold atoms, Nat. Commun. **7**, 12479 (2016).

[71] Y. H. Chen, Z. C. Shi, J. Song, Y. Xia, and S. B. Zheng, Accelerated and noise-resistant generation of high-fidelity steady-state entanglement with Rydberg atoms, Phys. Rev. A **97**, 032328 (2018).

[72] Y. H. Chen, Z. C. Shi, J. Song, Y. Xia, and S. B. Zheng, Coherent control in quantum open systems: An approach for accelerating dissipation-based quantum state generation, Phys. Rev. A **96**, 043853 (2017).

[73] A. Ruschhaupt, X. Chen, D. Alonso, and J. G. Muga, Optimally robust shortcuts to population inversion in two-level quantum systems, New J. Phys. **14**, 093040 (2012).

[74] P. Treutlein *et al.*, Quantum information processing in optical lattices and magnetic microtraps, Fortschr. Phys. **54**, 702 (2006).

[75] L. Sárkány, P. Weiss, H. Hattermann, and J. Fortágh, Controlling the magnetic-field sensitivity of atomic-clock states by microwave dressing, Phys. Rev. A **90**, 053416 (2014).

[76] T. Niemczyk *et al.*, Circuit quantum electrodynamics in the ultrastrong-coupling regime, Nat. Phys. **6**, 772 (2010).

[77] B. Peropadre, P. Forn-Díaz, E. Solano, and J. J. García-Ripoll, Switchable Ultrastrong Coupling in Circuit QED, Phys. Rev. Lett. **105**, 023601 (2010).

[78] J. R. Johansson, G. Johansson, C. M. Wilson, and F. Nori, Dynamical Casimir Effect in a Superconducting Coplanar Waveguide, Phys. Rev. Lett. **103**, 147003 (2009).

[79] J. R. Johansson, G. Johansson, and F. Nori, Optomechanical-like coupling between superconducting resonators, Phys. Rev. A **90**, 053833 (2014).

[80] P. D. Nation, J. R. Johansson, M. P. Blencowe, and F. Nori, Colloquium: Stimulating uncertainty: Amplifying the quantum vacuum with superconducting circuits, Rev. Mod. Phys. **84**, 1 (2012).

[81] Z. L. Xiang, S. Ashhab, J. Q. You, and F. Nori, Hybrid quantum circuits: Superconducting circuits interacting with other quantum systems, Rev. Mod. Phys. **85**, 623 (2013).

[82] J. Q. You, Y. X. Liu, C. P. Sun, and F. Nori, Persistent single-photon production by tunable on-chip micromaser with a superconducting quantum circuit, Phys. Rev. B **75**, 104516 (2007).

[83] Y. X. Liu, J. Q. You, L. F. Wei, C. P. Sun, and F. Nori, Optical Selection Rules and Phase-Dependent Adiabatic State Control in a Superconducting Quantum Circuit, Phys. Rev. Lett. **95**, 087001 (2005).

[84] J. Q. You and F. Nori, Atomic physics and quantum optics using superconducting circuits, Nature **474**, 589 (2011).

[85] X. Gu, A. F. Kockum, A. Miranowicz, Y.-X. Liu, and F. Nori, Microwave photonics with superconducting quantum circuits, Phys. Rep. **718-719**, 1 (2017).

[86] K. W. Murch, S. J. Weber, K. M. Beck, E. Ginossar, and I. Siddiqi, Reduction of the radiative decay of atomic coherence in squeezed vacuum, Nature **499**, 62 (2013).

[87] M. O. Scully and M. S. Zubairy, *Quantum Optics* (Cambridge University Press, Cambridge, England, 1997).

[88] *Quantum Squeezing*, edited by P. D. Drummond and Z. Ficek (Springer, Berlin, 2004).

[89] L.-A. Wu, M. Xiao, and H. J. Kimble, Squeezed states of light from an optical parametric oscillator, J. Opt. Soc. Am. B **4**, 1465 (1987).

[90] R. E. Slusher, L. W. Hollberg, B. Yurke, J. C. Mertz, and J. F. Valley, Observation of Squeezed States Generated by Four-Wave Mixing in an Optical Cavity, Phys. Rev. Lett. **55**, 2409 (1985).